Counterion Penetration and Effective Electrostatic Interactions in Solutions of Polyelectrolyte Stars and Microgels

A. R. Denton*

Department of Physics, North Dakota State University, Fargo, ND, 58105-5566

(Dated: May 19, 2004)

Abstract

Counterion distributions and effective electrostatic interactions between spherical macroions in polyelectrolyte solutions are calculated via second-order perturbation (linear response) theory. By modelling the macroions as continuous charge distributions that are permeable to counterions, analytical expressions are obtained for counterion profiles and effective pair interactions in solutions of star-branched and microgel macroions. The counterions are found to penetrate stars more easily than microgels, with important implications for screening of bare macroion interactions. The effective pair interactions are Yukawa in form for separated macroions, but are softly repulsive and bounded for overlapping macroions. A one-body volume energy, which depends on the average macroion concentration, emerges naturally in the theory and contributes to the total free energy.

PACS numbers: 82.70.Dd, 82.45.-h, 05.20.Jj

*Electronic address: alan.denton@ndsu.nodak.edu

I. INTRODUCTION

Polyelectrolytes (PEs) are ionizable polymers that dissolve in a polar solvent, such as water, by dissociating into polyvalent macroions and small oppositely-charged counterions [1]. Electrostatic interactions between macroions, mediated by surrounding microions (counterions and salt ions), contribute to the unique macroscopic properties of PE solutions, which are the basis of many industrial applications involving polymer-water systems [2]. Common synthetic examples of PEs are polyacrylic acid, used in gels and rheology modifiers, and polystyrene sulfonate, a component of reverse osmosis membranes. Naturally occurring examples are biopolymers, such as DNA, proteins, and starches. Colloidal in size, PEs are also routinely added as flocculants and stabilizers to colloidal suspensions, such as foods and water-based paints [3, 4]. Depending on PE concentration, adsorption or grafting of PE chains onto surfaces of colloidal particles can either induce flocculation, by bridging particles, or impart electrosteric stabilization.

Conformations of PE macroions and electrostatic interactions between macroions are strongly influenced by the distribution of microions. If dispersed in solution, microions act to screen the bare Coulomb interactions between ionized monomers. If condensed on the macroion chains, microions may reduce the macroion charge [5]. Linear PE chains whose monomers are sufficiently weakly interacting – either because weakly charged or because of strong microion screening or condensation – may form random-walk coils with roughly spherical conformation. With increasing charge and screening length, linear chains stretch into non-spherical conformations because of electrostatic repulsion between ionized monomers [6, 7]. The extent of elongation depends on the chain charge density, salt concentration, and solvent quality. Highly charged chains in good solvents (*e.g.*, DNA in water) often form stiff rod-like macroions, whose effective interactions and complex phase behavior (such as bundling) have been widely studied [8, 9]. In poor solvents, sufficiently highly charged chains may form necklaces of compact globules joined by narrow threads, as predicted by theory [10] and confirmed by simulation [11].

Although many common PEs are linear, other topologies can be readily synthesized. Examples are stars, microgels, micelles, and brushes. Star polymers [12] consist of chains chemically grafted or adsorbed to a common microscopic core. Microgels are mesoscopic

polymer networks, synthesized by polymerization in microemulsion [13]. Micelles are formed by association of charged diblock (amphiphilic) copolymers [14]. Brushes are formed by grafting PE chains onto a mesoscopic solid core [15]. Solutions of spherical stars, microgels, micelles, and brushes can be regarded as colloidal suspensions of soft macroions that are permeable to microions.

Electrostatic interactions in charged colloids have received much attention in recent years [16], motivated largely by anomalous phase behavior that is unexplained by the classic Derjaguin-Landau-Verwey-Overbeek (DLVO) theory [17]. Most studies have been restricted, however, to hard, impermeable macroions. The objectives of this paper are first, to explore implications of microion penetration for screening of effective electrostatic interactions between spherical macroions, and second, to lay a foundation for future studies of thermodynamic phase behavior of PE solutions. Our approach is based on a recently-proposed theory of effective interactions in charged colloids [18], which we adapt here from hard to penetrable macroions and apply to spherical star-branched and microgel macroions.

The remainder of the paper is organized as follows. Section II describes the assumed model of PE solutions. Section III reviews the theoretical approach, based on second-order perturbation (linear response) theory. Sections IV and V present analytical and numerical results for counterion profiles and effective interactions in bulk solutions of star and microgel macroions. Finally, Sec. VI closes with a summary and conclusions.

II. MODEL

Adapting the primitive model of ionic liquids [19], the model system comprises N_m spherical macroions, of radius a (diameter $\sigma = 2a$) and charge $-Ze$, and N_c point counterions of charge ze dispersed in an electrolyte solvent in a volume V at temperature T. Assuming, for simplicity, a symmetric electrolyte and equal salt and counterion valences, the electrolyte contains N_s point salt ions of charge ze and N_s of charge $-ze$. The microions thus number $N_+ = N_c + N_s$ positive and $N_- = N_s$ negative, for a total of $N_\mu = N_c + 2N_s$. Global charge neutrality in a bulk solution constrains average macroion and counterion number densities, $n_m = N_m/V$ and $n_c = N_c/V$, via $Zn_m = zn_c$. The polar solvent is treated as a continuum, characterized by dielectric constant ϵ that acts only to reduce Coulomb interactions between

ions.

The local number density profiles of counterions, $\rho_c(r)$, and of macroion monomers, $\rho_{\rm mon}(r)$, are modelled as spherically symmetric, continuous distributions. Spherical symmetry is a reasonable approximation, considering that equilibrium averaging over macroion orientations tends to smear out any anisotropy. Furthermore, discreteness of the charge distributions can be ignored if we restrict consideration to length scales exceeding the scale of discreteness.

In general, the counterions are distributed over three regions: (1) the immediate vicinity of the PE chains making up the macroions, (2) the region inside of the macroions but away from the chains, and (3) the region outside of the macroions. Counterions in the first two regions are trapped by the macroions, while those in the third region are free. Within the first region, the counterions may be either condensed on a chain or free to move along a tube surrounding a chain. These chain-localized counterions, whether condensed or mobile, tend to distribute uniformly along the chains to favor local charge neutrality. In our model, counterions in region (1) simply renormalize the effective macroion valence Z.

The detailed form of the monomer density profile depends on the macroion conformation. For star-branched macroions, Coulomb repulsion between charged monomers tends to stiffen and radially stretch the chains into a porcupine conformation [20]. We assume the ideal case of fully stretched chains and model the monomer density profile by $\rho_{\rm mon}(r \leq a) = Z/(4\pi a r^2)$, where r is the radial distance from the star's center. For microgel macroions, the dense network of chains is well approximated by a uniform monomer distribution, and is modelled here by $\rho_{\rm mon}(r \leq a) = 3Z/(4\pi a^3)$. This distribution may also approximate a weakly-charged linear PE chain with a spherical random-coil conformation, although a Gaussian distribution may then be more accurate. For both the star and microgel models, the monomer density profile is cut off sharply at the macroion surface: $\rho_{\rm mon}(r > a) = 0$.

III. THEORY

For the model PE solutions described above, the theoretical challenge is to predict the distributions of microions inside and outside of the macroions and the effective interactions between macroions. Following the same general strategy as applied previously to charged

colloids [18, 21], we reduce the multi-component mixture to an equivalent one-component system governed by effective interactions, which are approximated via perturbation theory. For clarity of presentation, we initially ignore salt ions. The Hamiltonian then decomposes into three terms:

$$H = H_m(\{\mathbf{R}\}) + H_c(\{\mathbf{r}\}) + H_{mc}(\{\mathbf{R}\},\{\mathbf{r}\}), \tag{1}$$

where $\{\mathbf{R}\}$ and $\{\mathbf{r}\}$ denote collective coordinates of macroion centers and counterions, respectively. The first term,

$$H_m = K_m + \frac{1}{2}\sum_{i\neq j=1}^{N_m} v_{mm}(|\mathbf{R}_i - \mathbf{R}_j|), \tag{2}$$

is the bare Hamiltonian for macroions with kinetic energy K_m that interact via the bare pair potential $v_{mm}(r)$ at center-center separation r. The form of $v_{mm}(r)$ depends on the macroion conformation and is specified in the Appendix. The second term in Eq. (1),

$$H_c = K_c + \frac{1}{2}\sum_{i\neq j=1}^{N_c} v_{cc}(|\mathbf{r}_i - \mathbf{r}_j|), \tag{3}$$

is the Hamiltonian for counterions with kinetic energy K_c that interact via the Coulomb pair potential $v_{cc}(r) = z^2e^2/\epsilon r$. The third term in Eq. (1),

$$H_{mc} = \sum_{i=1}^{N_m}\sum_{j=1}^{N_c} v_{mc}(|\mathbf{R}_i - \mathbf{r}_j|), \tag{4}$$

is the macroion-counterion interaction. For spherical macroions,

$$v_{mc}(r) \;=\; \begin{cases} \dfrac{-Zze^2}{\epsilon r}, & r > a \\ v_<(r), & r \leq a, \end{cases} \tag{5}$$

where the interaction inside a macroion, $v_<(r)$, depends on the macroion conformation and is specified in Sec. IV. For later reference, we note that Eq. (4) also may be expressed in the form

$$H_{mc} \;=\; \int \mathrm{d}\mathbf{R}\, \rho_m(\mathbf{R}) \int \mathrm{d}\mathbf{r}\, \rho_c(\mathbf{r}) v_{mc}(|\mathbf{R}-\mathbf{r}|), \tag{6}$$

where $\rho_m(\mathbf{R}) = \sum_{j=1}^{N_m}\delta(\mathbf{R}-\mathbf{R}_j)$ and $\rho_c(\mathbf{r}) = \sum_{j=1}^{N_c}\delta(\mathbf{r}-\mathbf{r}_j)$ are the macroion and counterion number density operators, respectively.

The mixture of macroions and counterions is formally reduced to an equivalent one-component system by tracing over counterion coordinates. Denoting counterion and

macroion (classical) traces by $\langle\ \rangle_c$ and $\langle\ \rangle_m$, respectively, the canonical partition function can be expressed as

$$\mathcal{Z} \;=\; \big\langle\langle\exp(-\beta H)\big\rangle_c\big\rangle_m \;=\; \big\langle\exp(-\beta H_{\rm eff})\big\rangle_m\,, \tag{7}$$

where $H_{\rm eff} = H_m + F_c$ is the effective one-component Hamiltonian, $\beta = 1/k_BT$, and

$$F_c \;=\; -\,k_BT\ln\Big\langle\exp\Big[-\beta(H_c+H_{mc})\Big]\Big\rangle_c \tag{8}$$

is the free energy of a nonuniform gas of counterions in the presence of the macroions.

At this stage, approximations are necessary for the counterion free energy. It is first convenient to convert the counterion Hamiltonian to the Hamiltonian of a classical one-component plasma (OCP) of counterions by adding to H_c, and subtracting from H_{mc}, the energy of a uniform compensating negative background [22], $E_b = -N_cn_c\hat{v}_{cc}(0)/2$, where $\hat{v}_{cc}(0)$ is the $k\to 0$ limit of the Fourier transform of $v_{cc}(r)$. Now regarding the macroions as an "external" potential for the OCP, we invoke perturbation theory [18, 19, 21] and write

$$F_c \;=\; F_{\rm OCP} \;+\; \int_0^1 {\rm d}\lambda\ \langle H'_{mc}\rangle_\lambda\,, \tag{9}$$

where $F_{\rm OCP} = -k_BT\ln\langle\exp[-\beta(H_c+E_b)]\rangle_c$ is the OCP free energy, the λ-integral charges the macroions, $H'_{mc} = H_{mc} - E_b$ represents the perturbing potential of the macroions acting on the counterions, and $\langle H'_{mc}\rangle_\lambda$ is the mean value of this potential in a solution of macroions charged to a fraction λ of their full charge. Further progress is facilitated by expressing H_{mc} [Eq. (6)] in terms of Fourier components:

$$\langle H_{mc}\rangle_\lambda \;=\; \frac{1}{V}\sum_{\mathbf{k}\neq 0}\hat{v}_{mc}(k)\hat{\rho}_m(-\mathbf{k})\,\langle\hat{\rho}_c(\mathbf{k})\rangle_\lambda + \frac{1}{V}\lim_{k\to 0}\left[\hat{v}_{mc}(k)\hat{\rho}_m(-\mathbf{k})\,\langle\hat{\rho}_c(\mathbf{k})\rangle_\lambda\right], \tag{10}$$

where $\hat{v}_{mc}(k)$ is the Fourier transform of Eq. (5) and where $\hat{\rho}_m(\mathbf{k}) = \sum_{j=1}^{N_m}\exp(i\mathbf{k}\cdot\mathbf{R}_j)$ and $\hat{\rho}_c(\mathbf{k}) = \sum_{j=1}^{N_c}\exp(i\mathbf{k}\cdot\mathbf{r}_j)$ are Fourier components of the macroion and counterion densities.

In first-order perturbation theory, the response of the counterion plasma to the macroions is ignored. Here we apply second-order perturbation (linear response) theory, in which the counterions are assumed to respond linearly to the macroion external potential:

$$\hat{\rho}_c(\mathbf{k}) \;=\; \chi(k)\hat{v}_{mc}(k)\hat{\rho}_m(\mathbf{k}), \qquad k\neq 0, \tag{11}$$

where $\chi(k)$ is the linear response function of the OCP. Note that the $k \to 0$ limit here, and in Eq. (10), must be treated separately, since the number of counterions, $N_c = \hat{\rho}_c(0)$, does not respond to the macroion charge, but rather is fixed by the constraint of global charge neutrality.

Upon combining Eqs. (9)-(11), the effective Hamiltonian can be recast in the form of the Hamiltonian of a pairwise-interacting system:

$$H_{\rm eff} \;=\; K_m \;+\; K_c \;+\; \frac{1}{2}\sum_{i\neq j=1}^{N_m} v_{\rm eff}(|\mathbf{R}_i - \mathbf{R}_j|) \;+\; E_0, \tag{12}$$

where $v_{\rm eff}(r) = v_{mm}(r) + v_{\rm ind}(r)$ is an effective macroion pair interaction that combines the bare macroion interaction with a microion-induced interaction

$$\hat{v}_{\rm ind}(k) \;=\; \chi(k)\left[\hat{v}_{mc}(k)\right]^2. \tag{13}$$

The final term in Eq. (12) is the volume energy, formally given by

$$E_0 \;=\; F_{\rm OCP} \;+\; \frac{N_m}{2}\lim_{r\to 0} v_{\rm ind}(r) \;+\; N_m \lim_{k\to 0}\left[-\frac{1}{2}n_m\hat{v}_{\rm ind}(k) + n_c\hat{v}_{mc}(k) + \frac{Z}{2z}n_c\hat{v}_{cc}(k)\right], \tag{14}$$

which is a natural by-product of the one-component reduction. Although independent of the macroion coordinates, the volume energy depends on the average macroion density and thus can influence thermodynamics.

The linear response function is proportional to the corresponding static structure factor, $S(k)$, which may be obtained from liquid-state theory [19]. In practice, the OCP is weakly correlated, with coupling parameter $\Gamma = \lambda_B/a_c \ll 1$, where $\lambda_B = \beta e^2/\epsilon$ is the Bjerrum length and $a_c = (3/4\pi n_c)^{1/3}$ is the counterion sphere radius. For example, for macroions of diameter $\sigma = 100$ nm, valence $Z = 100$, and volume fraction $\eta = (\pi/6)n_m\sigma^3 = 0.01$, in water at room temperature ($\lambda_B = 0.714$ nm), we find $\Gamma \simeq 0.014$. As for charged colloids [18, 21], we adopt the random phase approximation (RPA), which is accurate for weakly-coupled plasmas. The RPA equates the two-particle direct correlation function of the OCP to its exact asymptotic limit: $c^{(2)}(r) = -\beta v_{cc}(r)$. Using the Ornstein-Zernike relation, $S(k) = 1/[1 - n_c\hat{c}^{(2)}(k)]$, the linear response function then takes the analytical form

$$\chi(k) \;=\; -\,\beta n_c S(k) \;=\; -\,\frac{\beta n_c}{(1+\kappa^2/k^2)}, \tag{15}$$

where $\kappa = \sqrt{4\pi n_c z^2 \lambda_B}$ is the inverse Debye screening length. Note that since permeable macroions do not exclude counterions from their interiors, the excluded-volume corrections required for hard colloidal macroions [18] are not relevant here. With $\chi(k)$ specified, the counterion density can be explicitly determined from Eqs. (5) and (11) for a given macroion distribution (see Sec. IV). Finally, salt is easily introduced via additional microion response functions. In the process, the pair interaction and volume energy are unchanged, except for a redefinition of the screening constant as $\kappa = \sqrt{4\pi(n_c + 2n_s) z^2 \lambda_B}$, where n_s is the average number density of salt ion pairs.

It is worth noting the formal equivalence of the present theory to linearized Poisson-Boltzmann (DLVO) theory. Both are mean-field theories in the sense that they ignore fluctuations in microion distributions. An advantage of linear response theory, however, is that it encompasses the volume energy, which can be important for describing phase behavior [18, 21, 23–26]. Moreover, response theory can be straightforwardly generalized to incorporate nonlinear response, which entails both many-body effective interactions and corrections to the pair potential and volume energy [27]. In contrast, nonlinear Poisson-Boltzmann theory is practical only for the simple boundary conditions afforded by cell models. For simplicity, higher-order nonlinear effects are here ignored.

Equations (11)-(14) constitute the main formal expressions from linear response theory. Explicit calculations require specifying the counterion-macroion interaction $v_<(r)$ in Eq. (5) for specific macroion models. Below, we apply the theory to obtain analytical and numerical results for counterion profiles and effective interactions in bulk solutions of spherical star-branched and microgel macroions.

IV. ANALYTICAL RESULTS

A. Star Macroions

For our idealized model of a star-branched macroion with $1/r^2$ monomer density profile, Gauss's law gives the electric field as

$$E(r) = \begin{cases} -\dfrac{Ze}{\epsilon r^2}, & r > a \\ -\dfrac{Ze}{\epsilon a r}, & r \le a. \end{cases} \tag{16}$$

Integration over r yields the electrostatic potential energy between a star and a counterion:

$$v_{mc}(r) \;=\; \begin{cases} -\dfrac{Zze^2}{\epsilon r}, & r > a \\ -\dfrac{Zze^2}{\epsilon a}\,\left[1 - \ln\left(\dfrac{r}{a}\right)\right], & r \le a, \end{cases} \tag{17}$$

whose Fourier transform is

$$\hat{v}_{mc}(k) \;=\; -\,\frac{4\pi Zze^2}{\epsilon k^3 a}\,\mathrm{sinc}(ka), \tag{18}$$

with $\mathrm{sinc}(x) \equiv \int_0^x \mathrm{d}u\,\sin(u)/u$. We can now calculate the counterion number density around a single macroion in the dilute limit, where $\hat{\rho}_m(\mathbf{k}) = 1$. From Eqs. (11), (15), and (18), the Fourier component of the counterion density profile is given by

$$\hat{\rho}_c(k) \;=\; \frac{Z}{z}\,\frac{\kappa^2}{ka(k^2+\kappa^2)}\,\mathrm{sinc}(ka), \tag{19}$$

whose real-space form is

$$\rho_c(r) \;=\; \frac{Z}{z}\frac{\kappa}{8\pi a r}\,\begin{cases} 2\,\mathrm{sinhc}(\kappa a)\;e^{-\kappa r}, & r > a \\ \left[\mathrm{Ec}(\kappa a, \kappa r) + 2\,\mathrm{sinhc}(\kappa a)\right]\;e^{-\kappa r} \;-\; \mathrm{Ec}(-\kappa a, -\kappa r)\;e^{\kappa r}, & r \le a, \end{cases} \tag{20}$$

where

$$\mathrm{sinhc}(x) \;\equiv\; \int_0^x \mathrm{d}u\,\frac{\sinh(u)}{u} \;=\; \sum_{n=0}^{\infty}\frac{x^{2n+1}}{(2n+1)\cdot(2n+1)!} \tag{21}$$

and

$$\mathrm{Ec}(x_1, x_2) \;\equiv\; \int_{x_1}^{x_2}\mathrm{d}u\,\frac{e^u}{u} \;=\; \ln\left(\frac{x_2}{x_1}\right) + \sum_{n=1}^{\infty}\frac{x_2^n - x_1^n}{n\cdot n!}, \tag{22}$$

which can be efficiently computed from the first few terms of the rapidly converging series expansions. Approaching the macroion center, the counterion density profile varies more gradually than the $1/r^2$ macroion monomer density profile, diverging logarithmically, according to

$$\lim_{r\to 0}\rho_c(r) \;=\; \frac{Z\kappa^2}{4\pi a}\left[1 - \ln\left(\frac{r}{a}\right)\right]. \tag{23}$$

Integrating Eq. (20) over the spherical volume of the macroion yields the fraction of counterions inside a star:

$$f_{\mathrm{in}} \;=\; \frac{z}{Z}4\pi\int_0^a \mathrm{d}r\,r^2\rho_c(r) \;=\; 1 - \left(1 + \frac{1}{\kappa a}\right)\;e^{-\kappa a}\,\mathrm{sinhc}(\kappa a). \tag{24}$$

Note the clear predictions that (1) the counterion distribution is determined entirely by κa, or the dimensionless ratio of the macroion radius and the Debye screening length, and (2)

the fraction of counterions inside increases monotonically with κa. Thus, for fixed macroion radius, $f_{\rm in}$ increases with increasing macroion valence and concentration. This result is physically sensible: the shorter the screening length, the shorter the range of the counterion response, and thus the tighter the localization of counterions around the macroion centers.

From Eqs. (13) and (18), the induced electrostatic pair interaction is given by

$$\hat{v}_{\rm ind}(k) \;=\; -\,\frac{4\pi Z^2 e^2}{\epsilon}\,\frac{\kappa^2}{k^4 a^2 (k^2+\kappa^2)}\,{\rm sinc}^2(ka). \tag{25}$$

Fourier transforming, we obtain

$$v_{\rm ind}(r) \;=\; -\,\frac{2Z^2 e^2 \kappa^2 a^2}{\pi\epsilon r}\,\int_0^\infty {\rm d}x\,\frac{\sin(xr/a)}{x^3(x^2+\kappa^2 a^2)}\,{\rm sinc}^2 x. \tag{26}$$

For nonoverlapping stars, Eq. (26) can be reduced to the analytical form

$$v_{\rm ind}(r) \;=\; -\,\frac{Z^2 e^2}{\epsilon r} \;+\; \frac{Z^2 e^2}{\epsilon}\,\left[\frac{{\rm sinhc}(\kappa a)}{\kappa a}\right]^2\,\frac{e^{-\kappa r}}{r}, \qquad r > 2a. \tag{27}$$

Since nonoverlapping macroions interact via a bare Coulomb potential, $v_{mm}(r) = Z^2 e^2/\epsilon r$, the effective pair interaction for this case is

$$v_{\rm eff}(r) \;=\; \frac{Z^2 e^2}{\epsilon}\,\left[\frac{{\rm sinhc}(\kappa a)}{\kappa a}\right]^2\,\frac{e^{-\kappa r}}{r}, \qquad r > 2a. \tag{28}$$

Thus, at the level of linear response, nonoverlapping star macroions interact via an effective Yukawa (screened-Coulomb) pair potential. The screening constant, κ, in the potential depends on the total density of microions – inside and outside of the macroions – since all microions respond to the macroion charge. Note that the potential has the same r-dependence as the DLVO potential for hard colloidal macroions [4, 17],

$$v_{\rm DLVO}(r) \;=\; \frac{Z^2 e^2}{\epsilon}\,\left[\frac{\exp(\kappa a)}{1+\kappa a}\right]^2\,\frac{e^{-\kappa r}}{r}, \qquad r > 2a, \tag{29}$$

differing only in the macroion-size-dependent amplitude. For overlapping stars, the bare macroion interaction is somewhat more complex and is relegated to the Appendix.

Finally, from Eqs. (14), (18), (25), and (26), the volume energy is obtained as

$$\begin{aligned} E_0 \;&=\; F_{\rm OCP} \;-\; N_m \frac{Z^2 e^2 \kappa^2 a}{\pi\epsilon}\int_0^\infty {\rm d}x\,\frac{{\rm sinc}^2 x}{x^2(x^2+\kappa^2 a^2)} \\ &-\; (N_+ - N_-)\frac{k_B T}{2}. \end{aligned} \tag{30}$$

For weakly-coupled microion plasmas, the OCP free energy may be approximated by its ideal-gas limit:

$$F_{\rm OCP} \;=\; N_+[\ln(n_+\Lambda^3)-1] \;+\; N_-[\ln(n_-\Lambda^3)-1], \tag{31}$$

where Λ is the thermal wavelength. Note that if Z is allowed to vary (with counterion condensation), then the volume energy per macroion must be augmented by the self (Hartree) energy of a macroion: $U_H = Z^2e^2/\epsilon a$. The first term in Eq. (30), long recognized as important for phase behavior [1], represents the entropy of free counterions; the second term accounts for the cohesive electrostatic energy of microion-macroion interactions. The volume energy, analogous to its counterpart for charged colloids [18, 24, 25, 25], depends on the average macroion concentration and thus has the potential to influence phase behavior and other thermodynamic properties. Equations (20), (24), (28), and (30) are the main analytical results for star macroions.

It is important to emphasize that the present approach, while including the entropy of the counterions, neglects the configurational entropy of the macroions by assuming rigid (fully stretched) PE chains. Recently, Jusufi *et al.* [28] modelled pair interactions between PE stars by both molecular dynamics simulation and a variational free energy that incorporates chain flexibility. An important conclusion of their study is that pair interactions are dominated by counterion entropy. Our approach is complementary: while the macroion model neglects chain flexibility, which is reasonable at least for nonoverlapping stars, the linear response theory refines somewhat the modelling of the counterion distribution.

B. Microgel Macroions

For our model of microgel macroions, we apply exactly the same procedure as in Sec. IV A. The electric field of a uniformly-charged sphere is

$$E(r) \;=\; \begin{cases} -\dfrac{Ze}{\epsilon r^2}, & r > a \\ -\dfrac{Zer}{\epsilon a^3}, & r \le a, \end{cases} \tag{32}$$

which integrates to give the macroion-counterion interaction,

$$v_{mc}(r) \;=\; \begin{cases} -\dfrac{Zze^2}{\epsilon r}, & r > a \\ -\dfrac{Zze^2}{2\epsilon a}\left(3-\dfrac{r^2}{a^2}\right), & r \le a. \end{cases} \tag{33}$$

Equation (33) Fourier transforms to

$$\hat{v}_{mc}(k) \;=\; -\frac{12\pi Z z e^2}{\epsilon k^4 a^2}\left[\cos(ka)-\frac{\sin(ka)}{ka}\right], \tag{34}$$

which, when substituted into Eq. (11), yields the Fourier transform of the counterion density profile around a single macroion,

$$\hat{\rho}_c(k) \;=\; -\frac{Z}{z}\,\frac{3\kappa^2}{k^2a^2(k^2+\kappa^2)}\,\left[\cos(ka)-\frac{\sin(ka)}{ka}\right]. \tag{35}$$

The Fourier transform of Eq. (35) gives the real-space counterion density profile,

$$\rho_c(r) \;=\; \frac{Z}{z}\,\frac{3}{4\pi a^2 r}\,\begin{cases}\left[\cosh(\kappa a)-\dfrac{\sinh(\kappa a)}{\kappa a}\right]e^{-\kappa r}, & r>a\\ \dfrac{r}{a}-\left(1+\dfrac{1}{\kappa a}\right)e^{-\kappa a}\sinh(\kappa r), & r\le a,\end{cases} \tag{36}$$

which approaches a constant as $r \to 0$:

$$\rho_c(r=0) \;=\; \frac{Z}{z}\,\frac{3}{4\pi a^3}\,\left[1-(1+\kappa a)e^{-\kappa a}\right]. \tag{37}$$

Integration of Eq. (36) yields an analytical result for the internal fraction of counterions:

$$f_{\rm in} \;=\; 1-\frac{3}{\kappa a}\left(1+\frac{1}{\kappa a}\right)e^{-\kappa a}\left[\cosh(\kappa a)-\frac{\sinh(\kappa a)}{\kappa a}\right]. \tag{38}$$

Again the theory predicts a counterion distribution depending only on the ratio of macroion radius to screening length and an internal counterion fraction that increases monotonically with this ratio. This prediction may be compared with that of Oosawa's "two-phase" approximation [1], which assumes uniform (but differing) counterion concentrations inside and outside of the macroions. According to the latter approach, for spherical macroions with volume fraction η, the condition for equilibrium between free and bound counterions, in the absence of salt ions, is

$$\ln\left(\frac{f_{\rm in}}{1-f_{\rm in}}\right) \;=\; \ln\left(\frac{\eta}{1-\eta}\right) \;+\; Z\frac{\lambda_B}{a}(1-f_{\rm in})(1-\eta^{1/3}), \tag{39}$$

which must be solved numerically for $f_{\rm in}$. The predictions of Eqs. (38) and (39) are compared below in Sec. V.

Next, substituting Eq. (34) into Eq. (13), the induced pair interaction is

$$\hat{v}_{\rm ind}(k) \;=\; -\frac{36\pi Z^2 e^2}{\epsilon}\,\frac{\kappa^2}{k^6a^4(k^2+\kappa^2)}\,\left[\cos(ka)-\frac{\sin(ka)}{ka}\right]^2. \tag{40}$$

For nonoverlapping macroions, the Fourier transform of Eq. (40) is straightforward to evaluate and yields an effective pair interaction

$$v_{\rm eff}(r) \;=\; \frac{Z^2e^2}{\epsilon}\,\frac{9}{\kappa^4a^4}\,\left[\cosh(\kappa a)-\frac{\sinh(\kappa a)}{\kappa a}\right]^2\,\frac{e^{-\kappa r}}{r}, \qquad r>2a. \tag{41}$$

As for star macroions, a Yukawa form is predicted, but with a different amplitude. The case of overlapping macroions is left to the Appendix.

Finally, from Eqs. (14), (34), and (40), the volume energy is obtained as

$$\begin{aligned} E_0 \;&=\; F_{\rm OCP} \;-\; N_m\frac{3Z^2e^2}{\epsilon a}\left\{\frac{1}{5}-\frac{1}{2\kappa^2a^2}+\frac{3}{4\kappa^3a^3}\left[1-\frac{1}{\kappa^2a^2}+\left(1+\frac{2}{\kappa a}+\frac{1}{\kappa^2a^2}\right)e^{-2\kappa a}\right]\right\} \\ &-\; (N_+-N_-)\frac{k_BT}{2}. \end{aligned} \tag{42}$$

Equations (36), (38), (41), and (42) are the main analytical results for microgel macroions.

V. NUMERICAL RESULTS

The theory developed above can be applied to solutions of arbitrary ionic strength, under the assumption that the macroion PE chains remain stretched. In order to highlight the role of the counterions, we present numerical results for salt-free solutions. Within the model considered, the effect of salt is merely to increase the Debye screening constant. Furthermore, we consider the case of monovalent counterions ($z = 1$) in aqueous solutions at room temperature ($\lambda_B = 0.714$ nm). Figure 1 illustrates the form of the counterion number density profiles [Eqs. (20) and (36)] inside and outside of a macroion. Inside a star macroion the counterion density diverges logarithmically towards the center, while inside a microgel macroion $\rho_c(r)$ remains finite. Evidently, counterions penetrate stars more easily than they do microgels. This property is also reflected in the internal counterion fractions [Eqs. (24) and (38)], functions of κa only, which are shown in Fig. 2a. In Fig. 2b, we compare predictions of linear response theory [Eq. (38)] with those of Oosawa's two-phase approximation [Eq. (39)] for uniformly-charged spherical (microgel) macroions [1]. Both approaches qualitatively predict an increase in the fraction of bound counterions with increasing macroion concentration. However, linear response theory predicts a considerably more gradual accumulation of bound counterions than does the two-phase approximation.

Counterion penetration strongly influences screening of bare macroion interactions. The effective pair potentials, $v_{\rm eff}(r)$, and corresponding forces, $F(r) = -{\rm d}v_{\rm eff}(r)/{\rm d}r$, are shown in Figs. 3 and 4, respectively. Beyond overlap the effective interaction has Yukawa form, with the amplitude depending on the type of macroion. Figure 5 compares the variation of the macroion-size-dependent amplitude of $v(r > 2a)$ with the Debye screening constant for the two permeable macroions and for hard macroions. Evidently, the greater the permeability of the macroions to counterions, the weaker the amplitude of long-range repulsion. For overlapping macroions, the bare charge distribution combined with counterion penetration leads to softly repulsive interactions. Note that the interactions are bounded: they do not diverge as the macroions approach complete overlap. It must be emphasized that the effective interactions presented in Figs. 3 and 4 arise physically from electrostatic repulsion and counterion screening, but do not include steric interactions due to compression of overlapping chains [28].

VI. CONCLUSIONS

To summarize, we have applied second-order perturbation (linear response) theory to model solutions of spherical polyelectrolyte star-branched and microgel macroions. The theory predicts the counterion density profiles inside and outside of the macroions, effective interactions between pairs of macroions, and a one-body, density-dependent, volume energy that contributes to the total free energy of the system. The main conclusions are: (1) Counterions penetrate stars more easily than they do microgels. (2) Inside a star macroion, the density profile of mobile counterions varies more gradually than the macroion monomer density profile, diverging logarithmically toward the center. (3) The fraction of counterions trapped inside a macroion depends only on the ratio of macroion radius to Debye screening length and increases monotonically with this ratio. (4) Counterion screening significantly weakens the bare electrostatic pair interactions, which remain bounded up to complete overlap of macroions. (5) The effective pair interactions are softly repulsive for overlapping macroions and Yukawa in form for separated macroions, with amplitudes depending on the type of macroion.

It is important to point out some limitations of the theory. First, the linear response ap-

proximation limits applicability of the theory to dilute solutions of weakly charged macroions. The quantitative range of validity depends on the relative magnitudes of nonlinear corrections, including three-body and high-order interactions, in the perturbation expansion. The same techniques that have been used to analyze nonlinear response in charged colloids [27] can be applied to polyelectrolytes. Second, the mean-field approach taken here ignores fluctuations in the counterion distribution, which may be especially relevant for short-range interactions and multivalent counterions. Third, the neglect of chain flexibility restricts the theory to nonoverlapping macroions. This restriction may be reasonable for dilute solutions of sparsely separated macroions. However, for a sufficient concentration of macroions in a good solvent, chain elasticity and entropy must play a role. A unification of linear response theory and the variational theory of ref. [28] may then prove fruitful.

In principle, the predicted counterion profiles could be probed experimentally, *e.g.*, by neutron scattering, using isotopic labelling to contrast the PE chains and counterions. The macroion-macroion interactions may be less accessible to experiment. Conceivably, the solvent quality might be tuned to minimize the second virial coefficient between neutral monomers of overlapping macroions, effectively highlighting electrostatic interactions by masking any steric interactions. Comparisons of predicted and observed macroscopic properties will provide the most practical, if indirect, tests of the theory. Future applications will examine thermodynamic phase behavior, especially possible implications of the volume energy for the stability and structure of deionized solutions [13].

Acknowledgments

It is a pleasure to thank C. N. Likos and H. Löwen for helpful discussions and hospitality during a visit to the University of Düsseldorf, where parts of this work were completed. This work was supported by the National Science Foundation under Grant Nos. DMR-0204020 and EPS-0132289.

APPENDIX: INTERACTIONS BETWEEN OVERLAPPING MACROIONS

The bare Coulomb interaction between a pair of macroions at center-center separation r is given in general by

$$v_{mm}(r) \;=\; \frac{e^2}{\epsilon}\int \mathrm{d}\mathbf{r}' \int \mathrm{d}\mathbf{r}''\, \frac{\rho_{\mathrm{mon}}(\mathbf{r}')\rho_{\mathrm{mon}}(\mathbf{r}'')}{|\mathbf{r}'-\mathbf{r}''-\mathbf{r}|}. \tag{A.1}$$

For nonoverlapping macroions, spherical symmetry reduces the interaction to

$$v_{mm}(r) \;=\; \frac{Z^2e^2}{\epsilon r}, \qquad r > 2a. \tag{A.2}$$

For overlapping macroions, the six-dimensional integral in Eq. (A.1) may be reduced, by exploiting cylindrical symmetry and Gauss's law, to two-dimensional integrals, which in turn may be evaluated analytically. For star macroions, the result may be expressed piece-wise as follows:

$$\begin{aligned} v_{mm}(r) \;&=\; \frac{Z^2e^2}{2\epsilon a}\left\{\frac{9}{2} - \frac{7}{4}\frac{r}{a} - \frac{1}{2}\left[\left(3-\frac{a}{r}\right)\left(1-\frac{r}{a}\right) + \frac{r}{a}\ln\left(\frac{r}{a}\right)\right]\ln\left(\frac{a-r}{a}\right)\right. \\ &-\; \left.\frac{r}{2a}\int_{-1}^{a/r-1}\mathrm{d}x\,\frac{\ln(1+x)}{x} \;+\; \frac{r}{2a}\int_{1}^{a/r}\mathrm{d}x\,\frac{\ln(x-1)}{x}\right\}, \qquad 0 < r \le a \end{aligned} \tag{A.3}$$

$$\begin{aligned} v_{mm}(r) \;&=\; \frac{Z^2e^2}{2\epsilon a}\left\{\frac{9}{2} - \frac{7}{4}\frac{r}{a} - \frac{1}{2}\left[\left(3-\frac{a}{r}\right)\left(1-\frac{r}{a}\right) + \frac{r}{a}\ln\left(\frac{r}{a}\right)\right]\ln\left(\frac{r-a}{a}\right)\right. \\ &+\; \left.\frac{r}{2a}\int_{1-a/r}^{a/r}\mathrm{d}x\,\frac{\ln x}{1-x}\right\}, \qquad a < r \le 2a \end{aligned} \tag{A.4}$$

For computational purposes, the remaining integrals may be expressed as convergent series:

$$\begin{aligned} v_{mm}(r) \;&=\; \frac{Z^2e^2}{2\epsilon a}\left\{\frac{9}{2} - \frac{7}{4}\frac{r}{a} - \frac{1}{2}\left[\left(3-\frac{a}{r}\right)\left(1-\frac{r}{a}\right) + \frac{r}{a}\ln\left(\frac{r}{a}\right)\right]\ln\left(\frac{a-r}{a}\right)\right. \\ &+\; \frac{r}{2a}\left(\frac{1}{2}\left[\ln\left(\frac{r}{a}\right)\right]^2 - \frac{1}{2}\left[\ln\left(\frac{r}{a-r}\right)\right]^2 \;+\; \sum_{n=1}^{\infty}\frac{(r/a)^n - (r/(a-r))^n}{n^2}\right. \\ &+\; \left.\left.2\sum_{n=1}^{\infty}\frac{(r/(a-r))^{2n-1}-2}{(2n-1)^2}\right)\right\}, \qquad 0 < r \le a/2 \end{aligned} \tag{A.5}$$

$$\begin{aligned} v_{mm}(r) \;&=\; \frac{Z^2e^2}{2\epsilon a}\left\{\frac{9}{2} - \frac{7}{4}\frac{r}{a} - \frac{1}{2}\left[\left(3-\frac{a}{r}\right)\left(1-\frac{r}{a}\right) + \frac{r}{a}\ln\left(\frac{r}{a}\right)\right]\ln\left(\frac{a-r}{a}\right)\right. \\ &+\; \left.\frac{r}{2a}\left(\frac{1}{2}\left[\ln\left(\frac{r}{a}\right)\right]^2 \;+\; \sum_{n=1}^{\infty}\frac{(r/a)^n + (1-a/r)^n - 2}{n^2}\right)\right\}, \quad a/2 < r \le a \end{aligned} \tag{A.6}$$

$$v_{mm}(r) = \frac{Z^2e^2}{2\epsilon a}\left\{\frac{9}{2} - \frac{7}{4}\frac{r}{a} - \frac{1}{2}\left[\left(3-\frac{a}{r}\right)\left(1-\frac{r}{a}\right) + \frac{r}{a}\ln\left(\frac{r}{a}\right)\right]\ln\left(\frac{r-a}{a}\right)\right.$$
$$\left. - \frac{r}{2a}\sum_{n=1}^{\infty}\frac{(a/r)^n - (1-a/r)^n}{n^2}\right\}, \qquad a < r \leq 2a \tag{A.7}$$

For microgel macroions, the bare interaction may be expressed more compactly as

$$v_{mm}(r) = \frac{Z^2e^2}{\epsilon a}\left[\frac{6}{5} - \frac{1}{2}\left(\frac{r}{a}\right)^2 + \frac{3}{16}\left(\frac{r}{a}\right)^3 - \frac{1}{160}\left(\frac{r}{a}\right)^5\right], \qquad r \leq 2a. \tag{A.8}$$

Finally, the effective pair interaction between microgels, $v_{\rm eff}(r)$, is the sum of Eq. (A.8) and the induced interaction, obtained by Fourier transforming Eq. (40):

$$v_{\rm ind}(r) = -\frac{9Z^2e^2}{2\epsilon\kappa^4a^4r}\left\{\left(1 - e^{-\kappa r} + \frac{1}{2}\kappa^2r^2 + \frac{1}{24}\kappa^4r^4\right)\left(1 - \frac{1}{\kappa^2a^2}\right) + \frac{2}{\kappa a}e^{-2\kappa a}\sinh(\kappa r)\right.$$
$$+ \left[e^{-2\kappa a}\sinh(\kappa r) + 2\kappa^2ar + \frac{1}{3}\kappa^4(4a^3r + ar^3)\right]\left(1 + \frac{1}{\kappa^2a^2}\right) - \frac{2r}{a}\left(1 + 2\kappa^2a^2 + \frac{8}{15}\kappa^4a^4\right)$$
$$\left. - \frac{r^3}{3a^3}\left(\kappa^2a^2 + \frac{4}{3}\kappa^4a^4\right) - \frac{1}{720}\frac{\kappa^4}{a^2}r^6\right\}, \qquad r \leq 2a. \tag{A.9}$$

[1] F. Oosawa, *Polyelectrolytes* (Dekker, New York, 1971).

[2] *Polyelectrolytes*, ed. M. Hara (Dekker, New York, 1993).

[3] D. F. Evans and H. Wennerström, *The Colloidal Domain* (2nd ed.) (Wiley-VCH, New York, 1999).

[4] R. J. Hunter, *Foundations of Colloid Science* (Oxford, New York, 1986).

[5] H. Schiessel and P. Pincus, *Macromol.* **31**, 7953 (1998).

[6] P.-G. de Gennes, *Scaling Concepts in Polymer Physics* (Cornell, Ithaca, 1979).

[7] A. Yu. Grosberg and A. R. Khokhlov, *Statistical Physics of Macromolecules* (AIP, New York, 1994).

[8] M. J. Stevens, *Phys. Rev. Lett.* **82**, 101 (1999); B.-Y. Ha and A. J. Liu, *Phys. Rev.* E **60**, 803 (1999); F. J. Solis and M. Olvera de la Cruz, *Phys. Rev.* E **60**, 4496 (1999); A. Diehl, H. A. Carmona, and Y. Levin, *Phys. Rev.* E **64**, 011804 (2001);

[9] A. A. Kornyshev and S. Leikin, *Phys. Rev. Lett.* **82**, 4138 (1999); *Phys. Rev. Lett.* **86**, 3666 (2001); *J. Chem. Phys.* **107**, 3656 (1997); *ibid* **108**, 7035(E) (1998); H. M. Harreis, A. A. Kornyshev, C. N. Likos, H. Löwen, and G. Sutmann, *Phys. Rev. Lett.* **89**, 018301 (2002).

[10] A. V. Dobrynin, M. Rubinstein, and S. P. Obukhov, *Macromol.* **29**, 2974 (1996); A. V. Dobrynin and M. Rubinstein, *Macromol.* **32**, 915 (1999).

[11] U. Micka and K. Kremer, *Europhys. Lett.* **49**, 189-195 (2000); A. V. Lyulin, B. Dünweg, O. V. Borisov, and A. A. Darinskii, *Macromol.* **32**, 3264 (1999).

[12] C. N. Likos, H. Löwen, M. Watzlawek, B. Abbas, O. Jucknischke, J. Allgaier, and D. Richter, *Phys. Rev. Lett.* **80**, 4450 (1998).

[13] F. Gröhn and M. Antonietti, *Macromol.* **33**, 5938 (2000).

[14] P. Guenoun *et al. Phys. Rev. Lett.* **81**, 3872 (1998).

[15] X. Guo and M. Ballauff, *Phys. Rev.* E **64**, 051406 (2001).

[16] For recent reviews, see C. N. Likos, *Phys. Rep.* **348**, 267 (2001); L. Belloni, *J. Phys.: Condens. Matter* **12**, R549 (2000); J. P. Hansen and H. Löwen, *Annu. Rev. Phys. Chem.* **51**, 209 (2000).

[17] B. V. Derjaguin, L. Landau, *Acta Physicochimica* (USSR) **14**, 633 (1941); E. J. W. Verwey,

J. T. G. Overbeek, *Theory of the Stability of Lyophobic Colloids* (Elsevier, Amsterdam, 1948).

[18] A. R. Denton, *J. Phys.: Condens. Matter* **11**, 10061 (1999); A. R. Denton, *Phys. Rev.* E **62**, 3855 (2000).

[19] J.-P. Hansen and I. R. McDonald, *Theory of Simple Liquids*, 2^{nd} edition (Academic, London, 1986).

[20] P. Pincus, *Macromol.* **24**, 2912 (1991).

[21] M. J. Grimson and M. Silbert, *Mol. Phys.* **74**, 397 (1991); E. Canessa, M. J. Grimson, and M. Silbert, *Mol. Phys.* **64**, 1195 (1988); in *Strongly Coupled Plasma Physics*, ed. S. Ichimaru (Elsevier/Yamada Science Foundation, 1990), p. 675.

[22] Although the background energy, E_b, is strictly infinite in the idealized case of point counterions, its addition and subtraction formally cancel corresponding infinities in H_c [Eq. (3)] and H_{mc} [Eq. (4)].

[23] R. van Roij and J.-P. Hansen, *Phys. Rev. Lett.* **79**, 3082 (1997).

[24] H. Graf and H. Löwen, *Phys. Rev.* E **57**, 5744 (1998).

[25] R. van Roij, M. Dijkstra, and J. P. Hansen, *Phys. Rev.* E **59**, 2010 (1999).

[26] P. B. Warren, *J. Chem. Phys.* **112**, 4683 (2000).

[27] A. R. Denton, `xxx.lanl.gov/abs/cond-mat/0110096`.

[28] A. Jusufi, C. N. Likos, and H. Löwen, *Phys. Rev. Lett.* **88**, 018301 (2002); *J. Chem. Phys.* **116**, 11011 (2002).

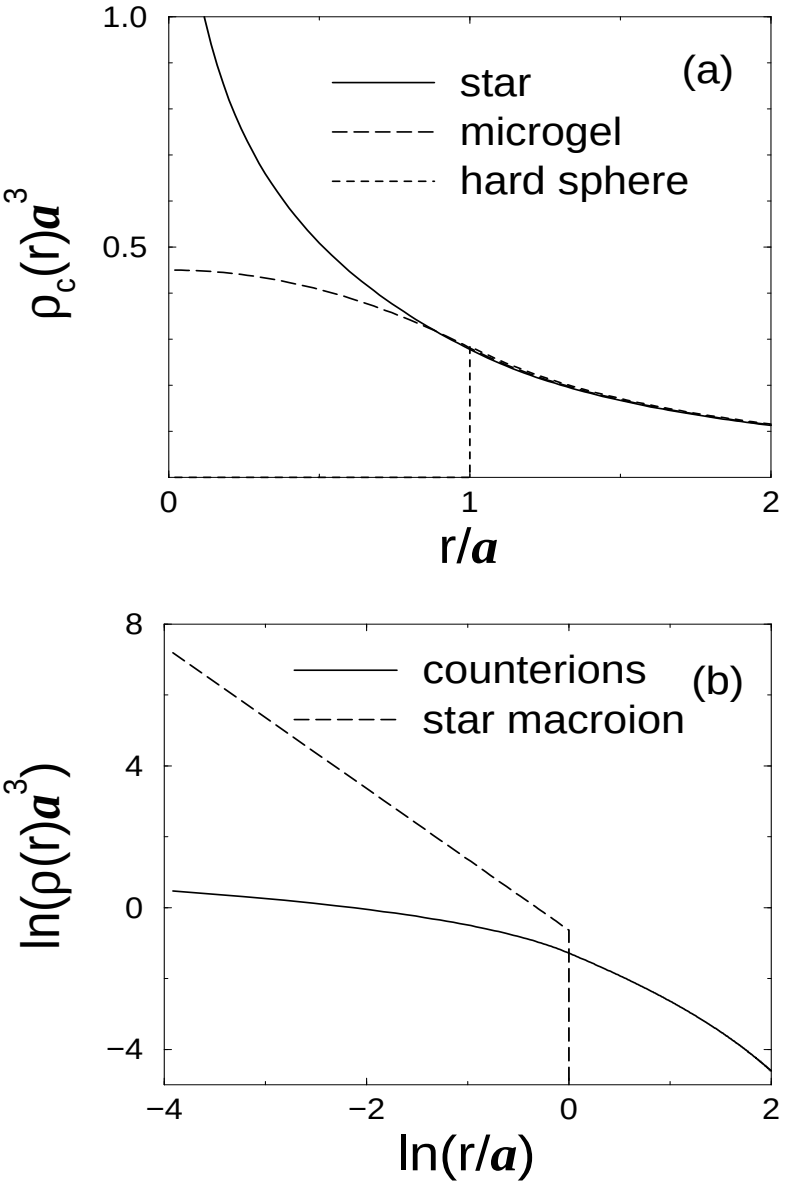

FIG. 1: (a) Counterion number density profiles [from Eqs. (20) and (36)] inside and outside of polyelectrolyte star and microgel macroions of diameter $\sigma = 100$ nm, valence $Z = 100$, and effective volume fraction $\eta = 0.01$, in water at room temperature ($\lambda_B = 0.714$ nm). The result for a hard-sphere macroion is shown for comparison. (b) Comparison of counterion and monomer density profiles for a star macroion on a log-log scale.

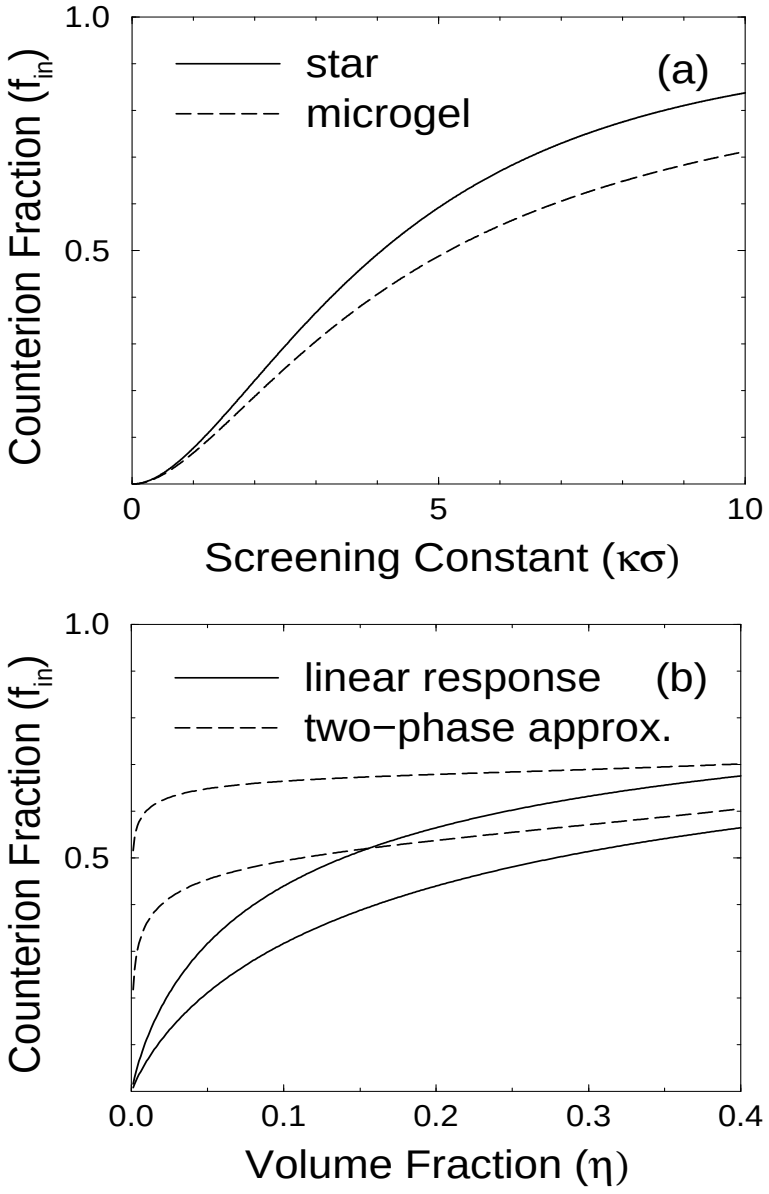

FIG. 2: (a) Fractions of counterions [from Eqs. (24) and (38)] inside polyelectrolyte star and microgel macroions vs. Debye screening constant κ. (b) Fraction of counterions inside a uniformly charged spherical macroion vs. effective macroion volume fraction as predicted by linear response theory (solid curves) and by the two-phase approximation of Oosawa [1] (dashed curves). For each case, the bottom curve corresponds to $Z\lambda_B/a = 8$ and the top curve to $Z\lambda_B/a = 16$.

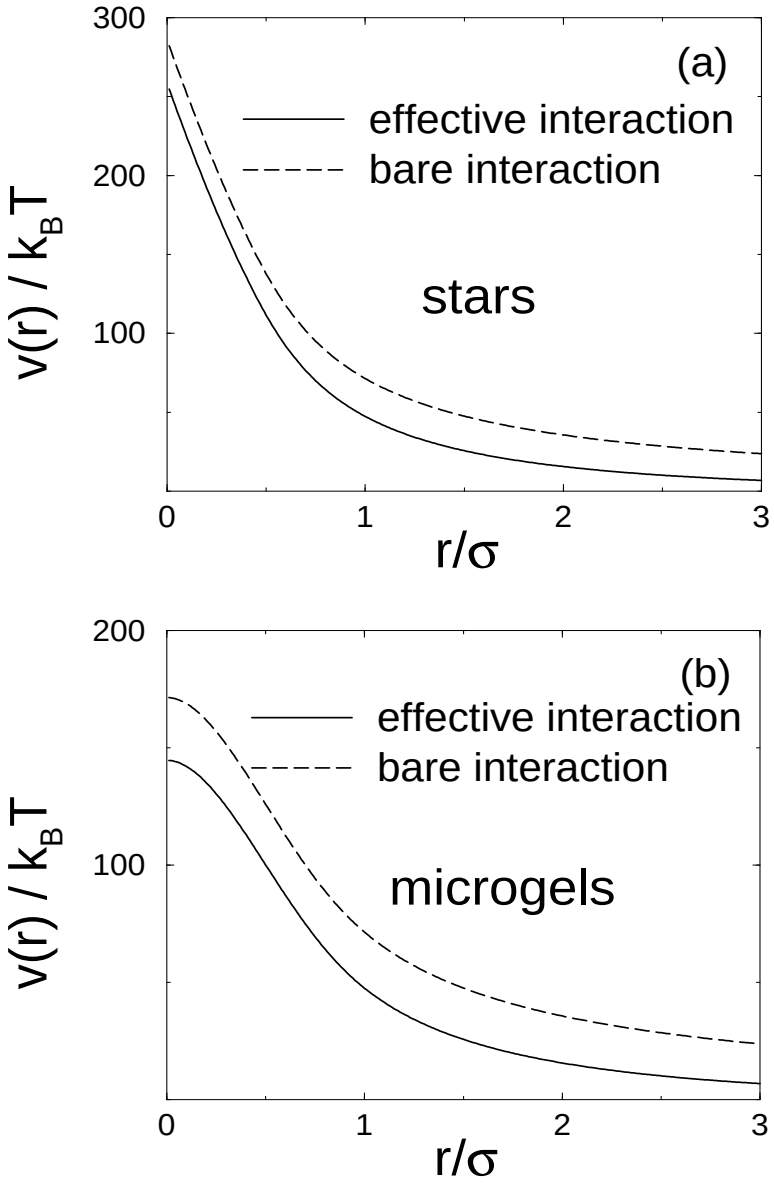

FIG. 3: Electrostatic interactions [from Eqs. (28) and (41)] between pairs of polyelectrolyte stars (a) and microgels (b). Dashed curves: bare interaction. Solid curves: effective (bare + induced) interaction. Parameters are the same as in Fig. 1. Beyond overlap ($r/\sigma > 1$), the interaction is Yukawa in form. For overlapping macroions ($r/\sigma < 1$), the soft repulsion remains finite at complete overlap ($r = 0$).

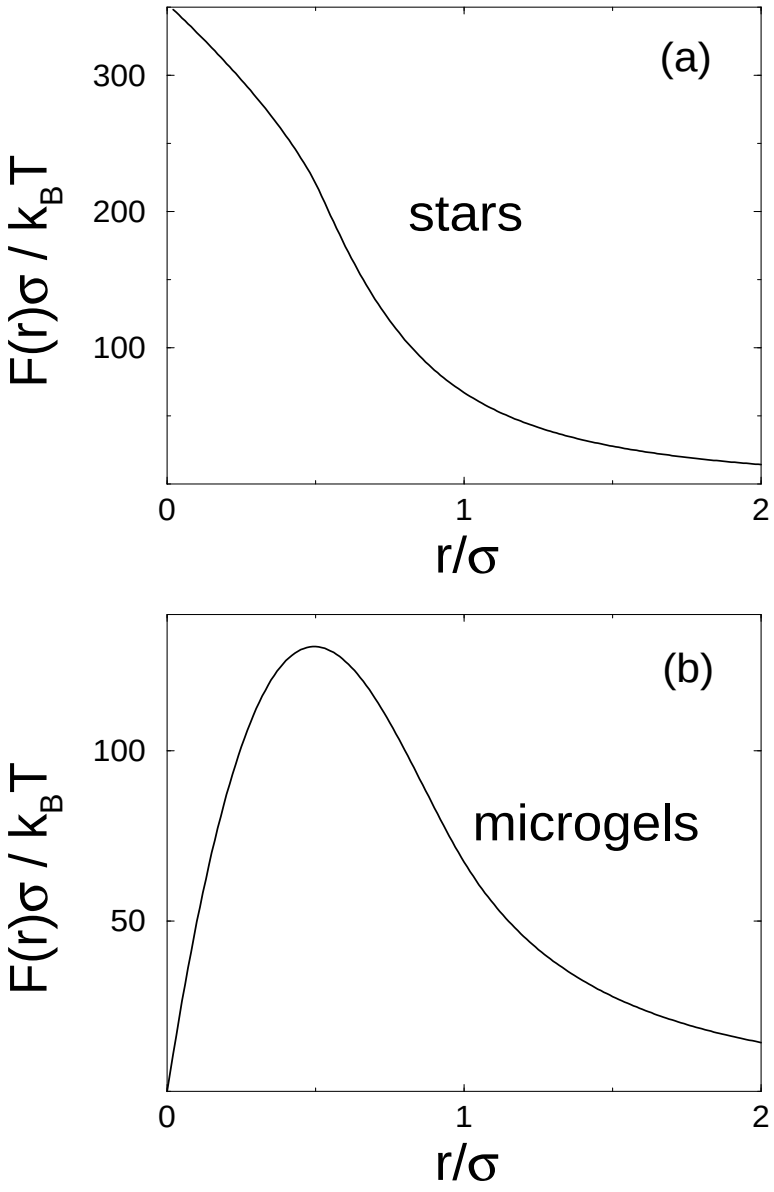

FIG. 4: Effective electrostatic forces between pairs of polyelectrolyte stars (a) and microgels (b), corresponding to the interaction potentials in Fig. 3. Parameters are the same as in Fig. 1.

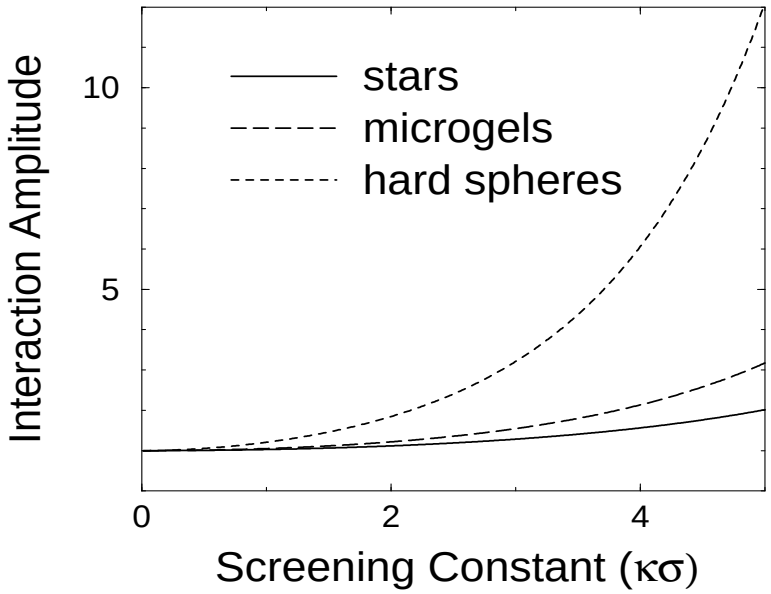

FIG. 5: Macroion-size-dependent amplitude of Yukawa effective electrostatic interactions [Eqs. (28), (29), and (41)] between pairs of nonoverlapping stars, microgels, and hard spheres vs. Debye screening constant, normalized to unity at $\kappa\sigma = 0$.